Single Cell Microgel Based Modular Bioinks for Uncoupled Cellular Micro- and Macroenvironments

Tom Kamperman, Sieger Henke, Albert van den Berg, Su Ryon Shin, Ali Tamayol, Ali Khademhosseini, Marcel Karperien, and Jeroen Leijten**

Native tissues are characterized by a multiscale modular design.[1] The cells and matrices within are spatially organized into repetitive 3D building blocks endowed with biochemical and biophysical cues having functional impact down to the single cell level.[2] In fact, these modules enable uncoupling of cellular and tissue micro- and macroenvironments, which is key to obtain the multifunctionality that is essential for proper tissue performance. Uncoupling the micro- and macroenvironments by integrating modularity is also expected to improve construct functionality of engineered tissues.[3] To this end, modularity has already been successfully incorporated in a number of bioengineering approaches, for example, by incorporating porogens or cell-laden microcarriers into an injectable biomaterial.[4] Here, we aim to engineer multifunctional tissues via a modular approach using bioink that comprises single-cell-laden microgels in an injectable macrogel. As cells covered by a thin layer of matrix are life's smallest functional units that can exist on their own, it is intuitive to create modular building blocks with single cell resolution. To this end, the encapsulation of single cells into micrometer-sized hydrogels, also called microgels, holds great promise. In particular, the combination of single-cell-laden microgels with distinct prepolymers would allow the development of modular bioinks that can create 3D multifunctional biomaterials of which the cellular micro- and macroenvironments are individually tunable. This biomimetic design is expected to provide biomaterials with the multifunctionality that is typically found in native tissues.

Various techniques have been exploited for the encapsulation of cells in microgels, including droplet microfluidics, bioprinting, micromolding, and stop-flow lithography.[5] Of these, droplet microfluidics has proven most suitable for the continuous high-throughput production of monodisperse spherical microgels. This approach has been widely used for the efficient encapsulation of multiple cells in microgels with a diameter as small as 100 µm.[6] By making use of the Poisson distribution, it has even been possible to encapsulate single cells into such microgels.[7] However, due to their size and low cell-to-volume ratio, these microgel particles have remained incapable of acting as modular building blocks for the creation of tissues with physiological cell concentrations. To address this need, subsequent studies with advanced approaches have attempted to encapsulate cells in microgels with sub-100 µm diameters. However, merely downsizing the microgels has typically been insufficient for enhancing cell encapsulation. Specifically, single cells take position at the droplet's water/oil interface resulting in partial cell encapsulation or even the "escape" of cells upon gelation.[8] Developing a facile fabrication strategy to produce single-cell-laden microgels that would be just micrometers larger than the cell size thus represents a key stepping stone for creating modular bioinks that can be used to engineer tissues with uncoupled cellular micro- and macroenvironments at a single cell level.

Here, we report on the development of such modular bioinks by enabling the high-throughput fabrication of microgels that fully encapsulate single cells, which are as small as 35 µm in diameter. In short, single-cell-laden microgels were produced by emulsifying a cell-laden hydrogel precursor solution in an immiscible oil phase using a microfluidic flow focusing device and subsequently photocrosslinking the resulting emulsion in a delay channel (**Figure 1**a). These microgels possess a vastly improved cell-to-volume ratio compared to microgels with a

T. Kamperman, Dr. S. Henke, Prof. M. Karperien, Dr. J. Leijten
Department of Developmental BioEngineering
MIRA Institute for Biomedical Technology and Technical Medicine
University of Twente
Drienerlolaan 5, 7500AE Enschede, The Netherlands
E-mail: h.b.j.karperien@utwente.nl; j.c.h.leijten@utwente.nl

Prof. A. van den Berg
BIOS Lab on a Chip group
MESA+ Institute for Nanotechnology
MIRA Institute for Biomedical Technology and Technical Medicine
University of Twente
7500AE Enschede, The Netherlands

Dr. S. R. Shin, Dr. A. Tamayol, Prof. A. Khademhosseini, Dr. J. Leijten
Biomaterials Innovation Research Center
Brigham and Women's Hospital
Harvard Medical School
02139 Cambridge, MA, USA

Dr. S. R. Shin, Dr. A. Tamayol, Prof. A. Khademhosseini, Dr. J. Leijten
Harvard-MIT Division of Health Sciences and Technology
Massachusetts Institute of Technology
02139 Cambridge, MA, USA

Dr. S. R. Shin, Dr. A. Tamayol, Prof. A. Khademhosseini
Wyss Institute for Biologically Inspired Engineering
Harvard University
02115 Boston, MA, USA

Prof. A. Khademhosseini
Department of Physics
King Abdulaziz University
21589 Jeddah, Saudi Arabia

Prof. A. Khademhosseini
Department of Bioindustrial Technologies
College of Animal Bioscience and Technology
Konkuk University
Hwayang-dong, Gwangjin-gu, Seoul 143-701, Republic of Korea

DOI: 10.1002/adhm.201600913

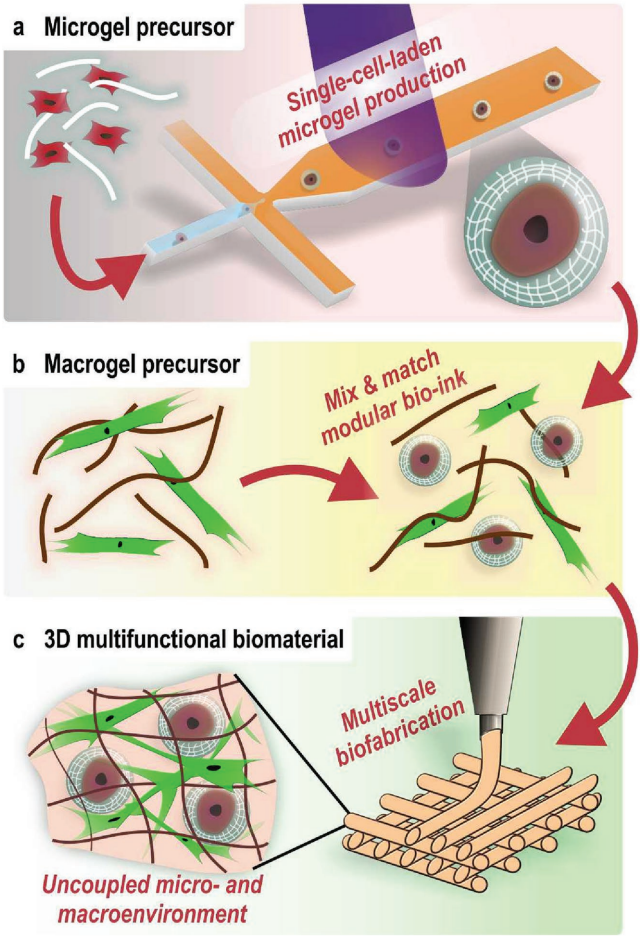

Figure 1. Schematic depiction of the creation of modular bioinks and fabrication of 3D multifunctional biomaterials, which possess uncoupled micro- and macroenvironments. a) Single-cell-laden microgels are produced by emulsifying and subsequent photocrosslinking cell-laden gel precursor microdroplets. b) Modular bioink is prepared by mixing the single-cell-laden microgels in a distinct injectable macrogel precursor. The macrogel's composition can be optimized independently from the microgels to provide the construct with multiple functions, for example, supporting the culture of different cell types. c) The injectable nature of the modular bioink makes it compatible with a variety of standard biofabrication techniques such as 3D bioprinting.

diameter of, e.g., 100 µm, making them highly suitable as high-resolution building blocks for modular tissue engineering. To demonstrate this, we incorporated the microgels into multiple distinct injectable macromaterials to effectively create several modular bioinks (Figure 1b), which were used for the biofabrication of various 3D constructs with an uncoupled micro- and macroenvironment (Figure 1c).

First, we aimed to encapsulate single cells into sub-50 µm microgels. To this end, we tested two different primary mammalian cell types (multipotent human mesenchymal stem cells (MSCs) and bovine chondrocytes) and selected polyethylene glycol diacrylate (PEGDA) as a model hydrogel. PEGDA allows for incorporation of a wide range of biomimetic elements and thus conforms as a template material for potential customization, which supports facile creation of user-defined cellular microenvironments.[9] Cell-laden PEGDA microdroplets were formed at a rate of ≈1 kHz using a microfluidic droplet generator (**Figure 2**a). Nozzle size was a key parameter in determining the hydrogel precursor droplet diameter, as we mainly utilized the flow focusing device in geometry-controlled or "squeezing" mode.[10] Therefore, the nozzle dimensions were minimized to 20 × 25 µm^2, thus only slightly larger than the average diameter of primary mammalian cells that we encapsulated (17 µm). A conventional crosslinking approach using only photoinitiator in the gel precursor phase, resulted in droplet coalescence and even expulsion of the cells from the microgels (Figure 2b). Indeed, cell-laden emulsions are relatively unstable due to the rapid adsorption of biomolecules and cells to the droplets' water/oil interface.[11] We implemented a dual photoinitiator system to achieve fast on-chip stabilization of the cell-laden droplets' water/oil interface, which was essential to prevent droplet coalescence and cell release (Figure 2c).[12] By dissolving photoinitiators in both the disperse water (0.1% Irgacure 2959) and the continuous oil (0.1% Irgacure 651) phases, we could encapsulate single cells in monodisperse PEGDA microgels with diameters between 35 and 40 µm in a robust and reproducible manner with good encapsulation quality, as measured by the relative position of the (semi-)encapsulated cell within the microgel (Figure 2d,e). The lower microgel diameter limit was determined by the size of the encapsulated single cells (10–35 µm). The microdroplets were photocrosslinked in an on-chip delay channel using an external UV-light source. To retrieve the microgels and allow their subsequent use, emulsions were broken by diluting the surfactant with hexadecane in the presence of serum-containing cell culture medium. The retrieved cell-laden microgels could be handled identically to cells in suspension. Importantly, more than 70% of the encapsulated cells (n = 220) remained viable throughout the encapsulation, gelation, and retrieval procedures, as shown by live/dead staining (Figure 2f). This indicated the cytocompatible nature of our microencapsulation strategy and supported its further use as a platform technology. Furthermore, this observation is in line with previously published reports, which crosslinked PEGDA off-chip into macroscale hydrogels.[13] It is of note that the incorporation of bioactive materials will support long-term cell viability and function. Regardless, we purposely exploited unmodified PEGDA, which is a universal bioinert template material that does not stimulate any specific cell functions by itself. Moreover, numerous biofunctional moieties to modify hydrogels such as PEGDA are readily available and compatible with our encapsulation platform, indeed enabling cell specific stimulation depending on the application of interest.[9] Scanning electron microscopy (SEM) revealed intact spherical microgels, indeed completely enclosing single cells (Figure 2g). This was corroborated by opening the microgels using focused ion beam (FIB) milling (Figure 2h). Furthermore, fluorescent confocal microscopy traced fluorescently labeled cells in the center of the microgels (Figure 2i). 3D visualization by z-stacking confocal images confirmed that the hydrogel indeed completely (i.e., without protrusions) enclosed the cells (Movie S1, Supporting Information). Together, our dual photoinitiator approach enabled droplet microfluidics technology to completely encapsulate single cells within a micrometer-thin hydrogel coating.

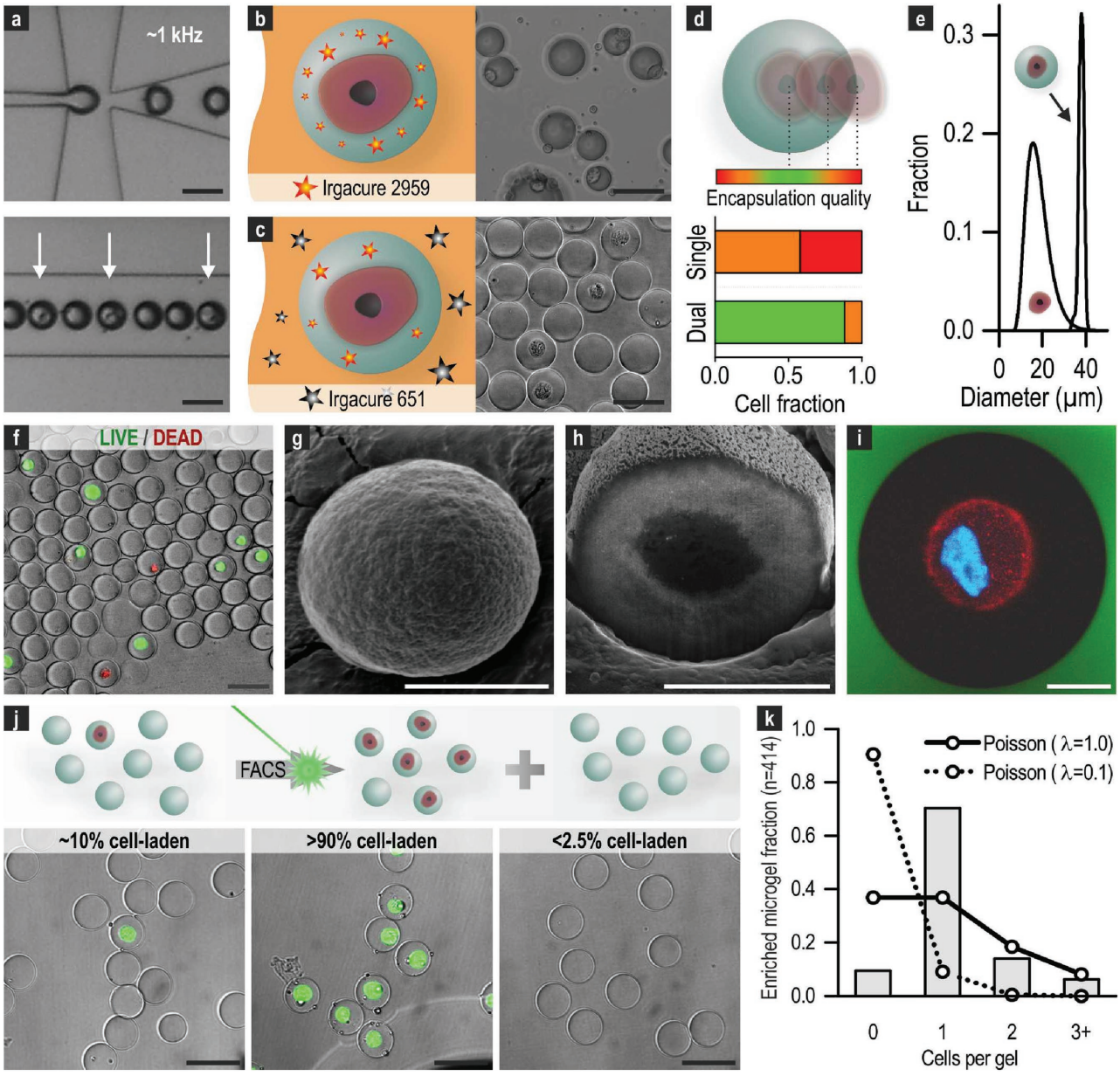

Figure 2. Single-cell-laden microgel production. a) High-throughput encapsulation of single cells (white arrows) in PEGDA precursor microdroplets using droplet microfluidics. b) Production of stable cell-laden microgels failed when using the gold standard single photoinitiator system, which relied on 0.1% Irgacure 2959 in the disperse phase. c) Proficient cell encapsulation into PEGDA microgels using a double photoinitiator system that contained 0.1% Irgacure 2959 in the disperse phase and 0.1% Irgacure 651 in the continuous phase. d) Histogram of the relative position of (semi-)encapsulated cells within microgels as a measure for cell encapsulation quality. e) Single-cell-laden microgels have a monodisperse size distribution with diameters between 35 and 40 μm, which is just larger than the single cells they encapsulate (10–35 μm). f) Live/dead staining of encapsulated chondrocytes post encapsulation. SEM images of a cell encapsulating microgel that is g) left intact or h) opened up using focused ion beam milling. i) Fluorescent confocal microscopy image demonstrating complete encapsulation of a single chondrocyte with stained membrane (red) and nucleus (blue) within a PEGDA microgel (black) residing in fluorescently labeled dextran solution (green). j) The cell-laden microgel fraction was enriched by selectively separating cell-laden microgels from microgels containing no cells using flow cytometry-based sorting. k) Distribution of encapsulated cells per microgel after flow cytometry-based enrichment (bars) and Poisson distributions (lines) with λ equal to 0.1 indicating the encapsulation yield of unsorted microgels and λ equal to 1.0 indicating the innate maximum single cell yield of random encapsulation. Black scale bars: 50 μm, white scale bars: 10 μm.

Although these data supported the proficient microencapsulation of cells, it had remained a random process that resulted in a mixed population of microgels containing no cell, a single cell, or multiple cells. Specifically, the number of encapsulated cells per microgel tightly fitted the Poisson distribution, which was dependent on the cell concentration of the gel precursor solution.[14] We aimed to overcome this limitation of random encapsulation and thereby to maximize the fraction of single-cell-laden modular building blocks. Although high-yield deterministic single cell encapsulation in culture medium droplets

has been shown using inertial focusing,[15] these forces are too weak to obtain longitudinal cell ordering in comparatively viscous fluids such as hydrogel precursor solutions. Instead, we exploited fluorescence-activated cell sorting (FACS) to obtain a fraction with maximal single cell yield and minimal amounts of microgels containing no cell or multiple cells (Figure 2j). Flow cytometry has already been proven to be compatible with high-throughput analysis and sorting of cell-laden microgels.[16,17] Here, we used this technique to break through the paradigm of Poisson-distributed cell encapsulation. To limit the number of multiple-cell-laden microgels, we encapsulated cells at a concentration of 9 million cells per mL of hydrogel precursor. Indeed, our encapsulation strategy resulted in a relatively high amount of microgels containing a single cell and a minimized amount of microgels containing multiple cells. Specifically, the number of encapsulated cells per microgel innately followed the Poisson distribution with lambda (λ) equal to 0.1 (Figure S1, Supporting Information). Consequently, we obtained a cell-laden microgel fraction of only ≈10%, while the majority (≈90%) of the microgels did not contain any cell (Figure 2j; Figure S2, Supporting Information). Using flow cytometry, microgels encapsulating fluorescently labeled cells could be readily distinguished from microgels containing no cells (Figure S3, Supporting Information). Labeled sorting increased the cell-laden microgel fraction from 10% to over 90% (Figure 2j; Figure S4, Supporting Information). Further analysis of the cell number per microgel revealed over 70% single-cell-laden microgels in the enriched population, thereby amply transcending the maximal single cell yield of a Poisson-distributed random cell encapsulation process with λ equal to 1, which is intrinsically limited to ≈37% (Figure 2k). As fluorescent labeling of cells might be suboptimal for some research applications and clinical translations, we explored label-free microgel sorting and demonstrated its feasibility. In particular, the presence of a cell within a microgel increased the forward-scattering and side-scattering of light, as compared to a microgel containing no cells (Figure S5, Supporting Information). Exploiting this feature, we were able to enrich the population of cell containing microgels from 10% to almost 70% in a label-free manner, with a single cell yield of 50% (Figure S6, Supporting Information). As cell expansion represents a major cost-determining factor in for example cell-based therapies, it is of importance to note that both sorting processes were nearly void of cell wastage. Almost none (<2.5%) of the cell-laden microgels were discarded, indicating the subtlety and precision of this enrichment method (Figure 2j; Figure S7, Supporting Information). It is expected that by selecting more stringent sorting parameters, the percentage of single-cell-laden microgels could be even further increased, although it might be at the expense of increased cell wastage. Altogether, by incorporating our current sorting strategy in the production process, we were able to generate single-cell-laden microgels with an encapsulation yield of 90% in a high-throughput manner.

A plethora of materials and processing techniques are currently being developed for the fabrication of cell-based constructs.[18] Conventionally, these biomaterials are archetypal a homogenous matrix in which individual cells are dispersed. In contrast, natural tissues are characterized by a multiscale hierarchical design, which provides tissues with spatially distinct compositions. Oversimplifying engineered tissues by neglecting this modular design limits their functionality. Here, we leveraged our microgels as building blocks to create modular bioinks that allow engineering of tissues with distinct material compositions at the micro- and macrolevel. This uncoupling enables novel material combinations and integration of multiple biochemical and biomechanical functions with single cell resolution. In order to expedite the translation of our multiscale modular approach, we have mixed our single cell building blocks with several clinically relevant materials and explored the compatibility of these bioinks with various commonly used biofabrication processes. Specifically, microgels were incorporated in macroconstructs of PEGDA using photolithography, dextran-tyramine conjugates using emulsification, collagen using injection molding, alginate/gelatin methacryloyl (GelMA) mixtures using 3D printing, and alginate using wet spinning and subsequent weaving (**Figure 3**a–e). Homogeneous distribution of microgels within distinct macromaterial was observed for all biomaterial combinations and fabrication techniques using fluorescent confocal microscopy. This mix-and-match approach successfully produced 3D biomaterials for all tested combinations and fabrication techniques, which demonstrates the universal applicability of this novel form of high-resolution modular tissue engineering.

An important design parameter of modular bioinks when engineering tissues is the concentration of microgels per macrogel volume. This ratio determines several of the construct's biological and biomechanical properties. For example, a low concentration of microgels allows for a more dominant role of the macrogel, potentially providing tissue constructs with, for example, excellent mechanical properties (**Figure 4**a). This creates novel opportunities for engineering tissues that are characterized by a low cell density such as cartilaginous tissues, which contain a low density of individual cell niches with a large volume of mechanically stable extracellular matrix. Conversely, a high microgel concentration enables the macrogel to act as a biological glue, indeed confining the specialized microniches in minimal spatial manner (Figure 4b). Importantly, the single-cell-laden microgel concentration also determines the cell seeding density of the construct. Although cell concentrations are tissue dependent, their physiological range lies mostly between 10^6 and 10^8 cells per cm^3 tissue.[19] Concerning this, we would like to highlight the drastic impact of single-cell-laden microgels' size on the maximum number of cells that can be seeded into a 3D construct. Therefore, we calculated the total number of cells in one cm^3 construct that contains only single-cell-laden microgels, as a function of microgel diameter. Importantly, we assumed that single-cell-laden microgels are produced with relatively low encapsulation yield (10%); a common strategy to prevent the formation of multicell microgels resulting from innate Poisson statistics.[14,17] Furthermore, we assumed a maximum sphere packing density of 75%, based on the theoretical limit of spheres packed in 3Ds.[20] Figure 4c clearly demonstrates that typically reported microgels with a diameter of 100 µm could barely result in 10^5 cells per cm^3 (black dashed line). Microgels with a diameter below 50 µm are required to reach natural densities of ≥10^6 cells per cm^3. Opportunely, combining our microencapsulation platform with flow cytometry-based enrichment even boosted the theoretical maximum cell seeding density of constructs composed of these

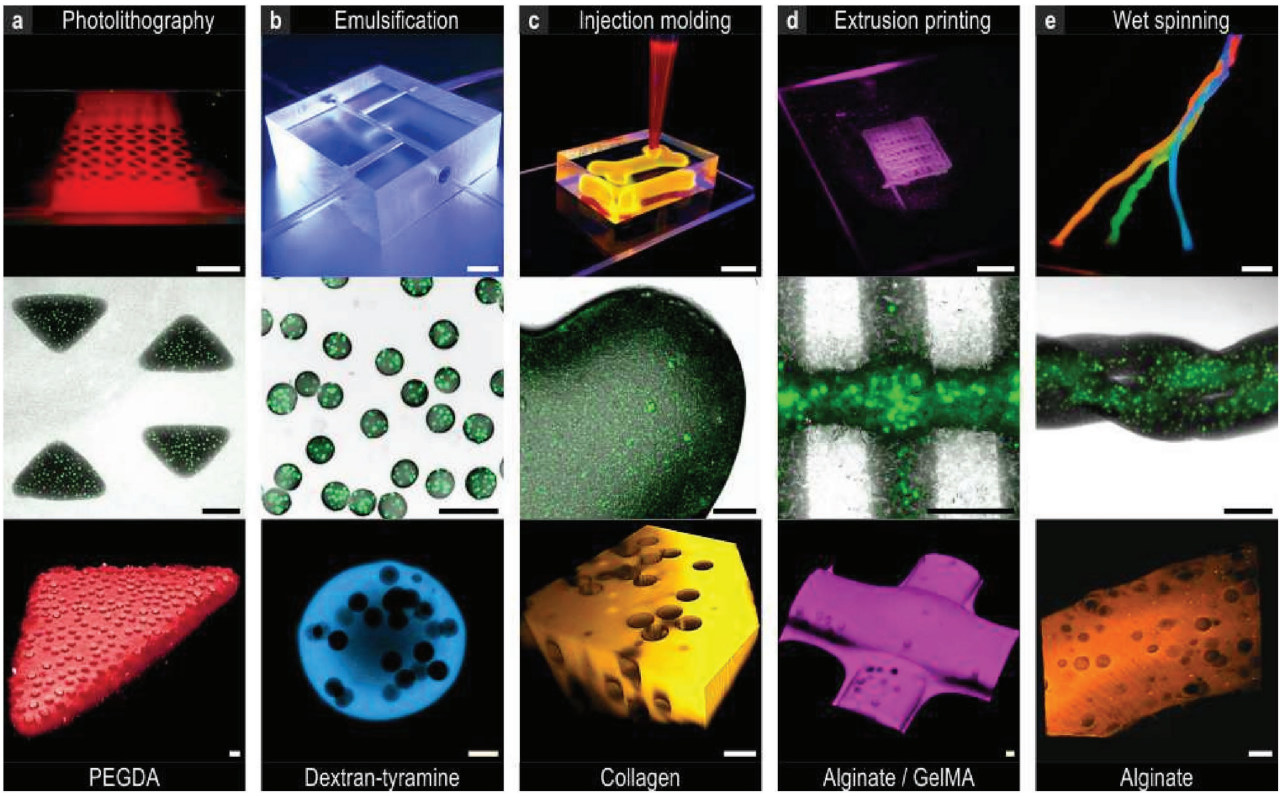

Figure 3. Biofabrication of 3D constructs using modular bioinks. Standard biofabrication techniques (top) were exploited for the production of 3D constructs (middle) that contained PEGDA microgels as modular building blocks incorporated into a variety of injectable macromaterials (bottom). Fluorescent (confocal) imaging confirmed the homogeneous distribution of microgels throughout the constructs. The constructs were fabricated by a) photopatterning PEGDA, b) emulsifying dextran-tyramine, c) injection molding collagen, d) extruding alginate/GelMA, or e) wet spinning and subsequent weaving alginate. Top scale bars: 5 000 µm, middle scale bars: 500 µm, bottom scale bars: 50 µm.

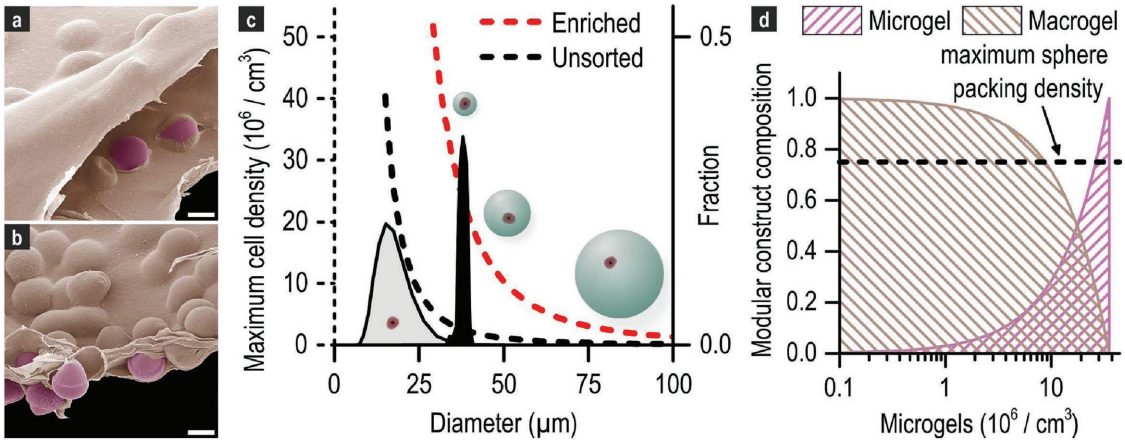

Figure 4. Effects of microgel concentration on modular construct composition. PEGDA microgels were seamlessly incorporated into an agarose bulk hydrogel at both a) low and b) high concentrations and imaged using SEM. SEM images were pseudo-colored, showing PEGDA in pink and agarose in beige. c) The maximum cell seeding density is determined by the microgel diameter (i.e., black dashed line). Importantly, microgels smaller than 50 µm are required to yield cell seeding densities above one million per cm^3 construct. Enriching the cell-laden microgel fraction using flow cytometry-based sorting tremendously increased the theoretical cell seeding density of a construct packed with single cell microgels (i.e., red dashed line) to more than 20 million cells per cm^3 of construct, compared to a mere 2 million in case of using unsorted single-cell-laden microgels of 38 µm. The size distributions of single cells and single-cell-laden microgels are indicated in black and gray, respectively. d) The microgel concentration determines the volume ratio of micro- and macromaterial. When using 38 µm single-cell-laden microgels at a typical concentration for tissue-engineered implants of one million per cm^3, the micromaterial merely makes up 1% of the total construct volume. Scale bars: 10 µm.

single cell building blocks to >10^7 per cm^3 (red dashed line). Attaining these cell concentrations enables the use of single-cell-laden microgels in cell-laden biomaterial-based therapies, which may require such high cell seeding concentrations to achieve proper clinical outcomes. Besides the cell seeding density argument, smaller single-cell-laden microgels are also favorable from a pharmacological perspective, as they are characterized by faster diffusion time of solutes (e.g., nutrients and cytokines) and relatively small gel to cell volume ratios, for example, maximizing screening efficiency (Figure S8, Supporting Information).

Another major opportunity of modular biomaterials lies in the straightforward reduction of growth factor amount that is commonly required for tissue engineering applications. Conventionally, cell-based tissue-engineered constructs are homogeneously endowed with a supraphysiological payload of growth factors, peptides, or small molecules. This is often necessitated by our desire to steer the encapsulated cells' proliferation, migration, or function. However, in clinical trials these bulk loads of, e.g., growth factors are frequently the main cause of adverse effects such as tissue inflammation, vessel leakage, and even cancer formation.[21] The modular nature of our bioinks allows for site-specific—or even cell-specific—growth factor incorporation in either the micro or macroenvironment, enabling considerable minimization of total growth factor amounts. To illustrate the significant potential of the modular bioink's uncoupled micro- and macroenvironments, we calculated the relative matrix composition of 1 cm^3 modular construct as a function of microgel number (Figure 4d). For example, by only administering cell-stimulating growth factors to the microgels in implants with a single-cell-laden microgel load of 10^6 per cm^3, the required amount of growth factors could be reduced by >99%. In short, the use of single cell microgel-based bioinks could reduce the amount of incorporated growth factor by two orders of magnitude while maintaining physiological concentrations around the cells. This may not only prevent potential adverse effects, but also lower therapy costs without affecting the biological performance of the construct, thus supporting clinical translation on several fronts.

Finally, we demonstrated that our modular bioinks integrate the functions of multiple biomaterials into a single 3D construct. In particular, we aimed to fabricate a 3D construct providing both biomaterial-based immunoprotection and vascularization. Although these two characteristics are not compatible in conventional approaches, using modular bioink both functions could be readily incorporated in a single construct through its uncoupled micro- and macroenvironments.

Currently, cell transplantations almost exclusively rely on autologous and allogeneic sources, which are typically only available in limited quantities.[22] Genetically modified xenogeneic sources could offer an alternative and are available in relatively copious quantities.[23] However, nonautologous cell transplantations are still hampered by the host-versus-graft immune response and therefore require constant immunosuppressive treatments. Shielding nonautologous cells from the host's immune system can be achieved by encapsulating the cells in a specific permselective microgel. PEGDA hydrogels have previously been demonstrated to render the construct with such immunoprotective properties.[24] However, PEGDA cannot be remodeled in vivo and thus impedes blood vessel invasion, host integration, and implant survival. A modular approach using PEGDA-based single cell building blocks inside a distinct biomaterial enables the engineering of a multifunctional tissue construct that provides both immunoprotective and proangiogenic functions. Using diffusion assays with fluorescently labeled dextran and proteins, we confirmed that micrometer-sized PEGDA gels provide similar immunoprotective capacity as the previously reported larger constructs (**Figure 5**a; Figure S9, Supporting Information). In particular, they blocked the penetration of molecules with a hydrodynamic diameter larger than ≈10 nm (Figure 5b). Besides controlling the cell's microenvironment, our bioink's multiscale modularity enables the independent engineering of the construct's macromaterial. Due to the spherical nature of the microgels, the macromaterial maintains an interconnected network. Therefore, it can function as a conduit for cellular ingrowth and thus act, for example, as a highway for vascularization, enabling all microgels to be located within micrometers of a vascular network. To demonstrate this, we formed a modular bioink composed of immunoprotective single cell PEGDA microgels, endothelial cells, MSCs, and proangiogenic fibrinogen macromaterial solution, which was solidified using thrombin to form 3D multifunctional constructs. Within one week of culturing these constructs, the angiogenic cells in the macromaterial assembled into a CD31-positive prevascular network that permeated throughout the construct (Figure 5c). We observed bridging and encapsulation of microgels by the endothelial network in the macromaterial (Figure 5d,e). The single-cell-laden microgels were seamlessly integrated within the macrogel, while maintaining their immunoprotective capacity, proving the construct's multifunctionality (Figure 5f,g). Importantly, confocal microscopy confirmed that none of the cells in the macromaterial penetrated any of the microgels, corroborating the existence of the immunoprotective microenvironments within a prevascularized macromaterial (Figure 5h). We leveraged this approach by coculturing different cell types in the uncoupled micro- and macroenvironments of these 3D multifunctional constructs. Specifically, MSCs were encapsulated in immunoprotective PEGDA microgels, which were then incorporated in endothelial cell and MSC containing fibrin (Figure 5i). In principle, this approach prevents exposure of the microencapsulated cells to the host's immunoglobulins, while preserving the diffusion of their nutrients, waste products, and signaling molecules, such as growth factors (Figure 5j). The microgels' small diameter enabled the vascular network to establish within micrometers of the microencapsulated cells, enabling fast response to cytokines in the blood, as well as unhampered diffusion of nutrients and waste, thereby abating the necrosis that is often observed in scaffolds offering immunoprotection.[25] Potentially, nonautologous cells encapsulated in an immunoprotective microenvironment can be utilized in a variety of standard transplantation procedures, such as stem cell therapies. In short, modular bioinks can simultaneously provide cell-centric microenvironments, for example, immunoprotection for nonautologous cells, as well as host-centric macroenvironments such as integration, anastomosis, and implant survival.

In summary, high-throughput microfluidics and flow cytometry-based sorting technologies enabled the production

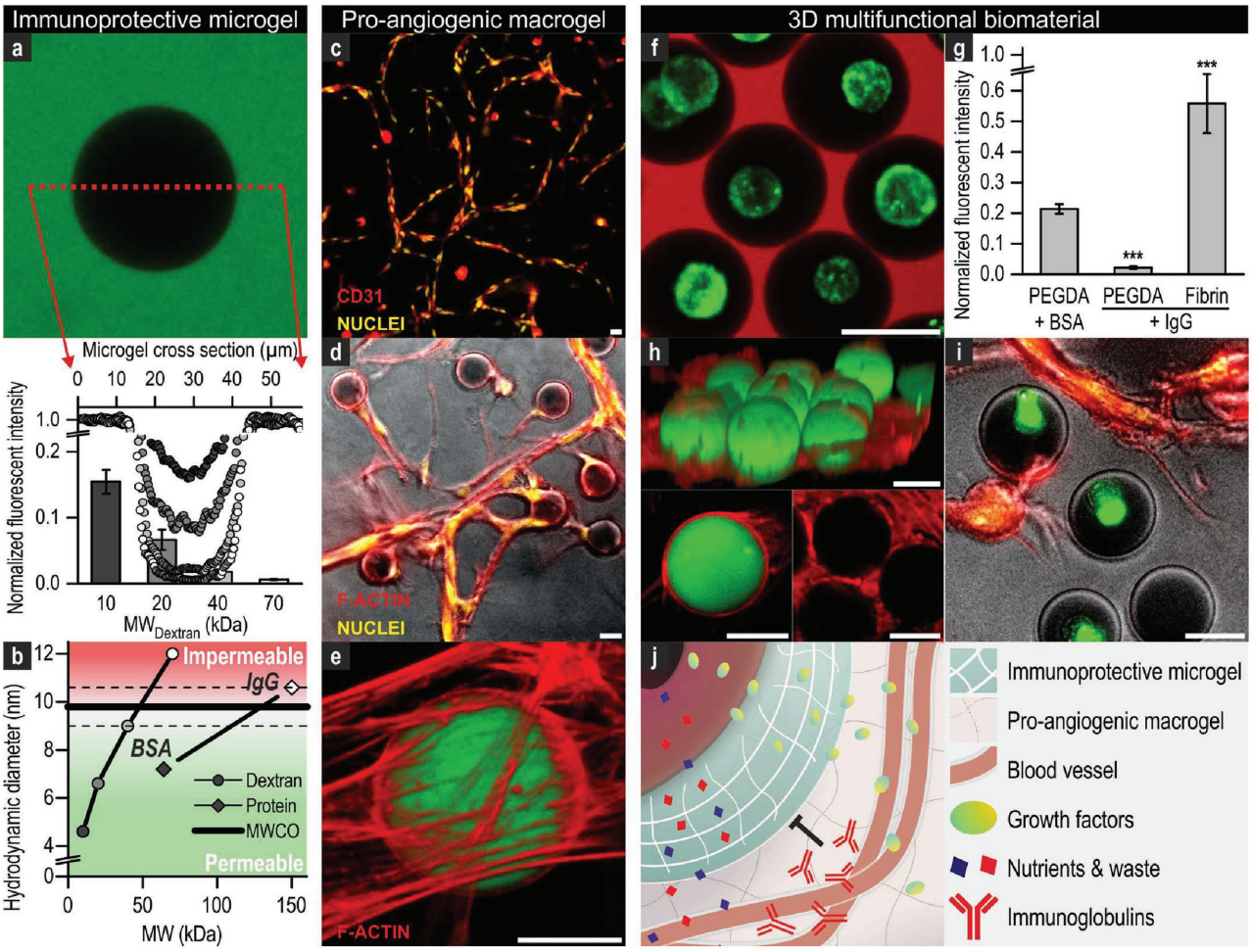

Figure 5. Multifunctional biomaterials with uncoupled micro- and macroenvironments fabricated using modular bioink. a) The micromaterial's permselectivity was determined by measuring fluorescent intensities across PEGDA microgels (circles) using fluorescent confocal microscopy after 6 d of incubation in solutions with fluorescently labeled dextrans of various molecular weights, with darker data points representing lower molecular weights. The bars represent the average intensities of the microgels' centers. b) Dextran and protein diffusion assays indicated that the microgels are permeable to molecules with a hydrodynamic diameter below 10 nm. Multifunctional modular biomaterial was produced by embedding the immunoprotective PEGDA microgels in a proangiogenic fibrin macrogel. The endothelial cells in the macromaterial formed a c) CD31-positive interconnected network that d) bridged and e) encapsulated the microgels. f) Single cell (green) PEGDA microgels seamlessly integrated with fibrin macrogel, while maintaining immunoprotective properties, demonstrated by impermeability to fluorescently labeled 70 kDa dextran (red) and g) IgG, while allowing permeation of BSA. h) Confocal imaging confirmed that endothelial cells spread throughout the macrogel, but did not penetrate any of the microgels. i) Proof-of-concept of a 3D multifunctional modular biomaterial with an uncoupled cellular micro- and macroenvironment where microencapsulated MSCs (green) are immunoprotected, while cocultured with endothelial cells and MSCs (red with yellow nuclei) in a proangiogenic macroenvironment. j) Schematic depicting the concept of a multifunctional biomaterial that contains immunoprotective single-cell-laden microgels embedded in a proangiogenic macromaterial. ***$p < 0.001$. Scale bars: 25 μm.

of small (<40 μm) single-cell-laden microgels with near pure (>90%) encapsulation yield. These microgels could be mixed-and-matched with numerous biomaterials to create multiple modular bioinks, which were proven to be compatible with various standard biofabrication techniques to fabricate 3D multifunctional biomaterials. Uniquely, this approach could exploit the individual materials' advantages, while limiting or omitting their drawbacks. Specifically, the use of modular bioinks enabled uncoupled optimization of the biomaterials bulk and the cell's microenvironment with a single cell resolution, which was thus far impossible. Finally, the modular bioink-based approach's throughput, versatility, straightforward, and cost-effective nature primes it for rapid adoption in a myriad of clinically relevant applications.

Experimental Section

A detailed description of the experimental section is included in the Supporting Information.

Cell-Laden Microgel Production: Bovine chondrocytes were isolated from patellar-femoral groove cartilage of calf legs and cultured as previously reported.[26] Human MSCs were isolated from fresh bone marrow samples and cultured as previously described.[27] The use of patient material was approved by the local ethical committee of the

Medisch Spectrum Twente and informed written consent was obtained for all samples. Microfluidic chips with 25.8 µm high structures were fabricated from polydimethylsiloxane and glass using standard soft lithography techniques. Aquapel was flown through the chip to ensure channel wall hydrophobicity. To produce the cell-laden microgels, culture medium containing 10% (w/v) PEGDA 3400, 0.1% (w/v) Irgacure 2959, 33% (v/v) Percoll, and 9 million cells per mL was emulsified in hexadecane supplemented with 1% (v/v) Span 80, 0.1% (w/v) Irgacure 651, and 0.3% (v/v) N-Vinylpyrrolidone on-chip, using low pressure syringe pumps. Microdroplets were cured using 365 nm UV-light on-chip (≈5 s at ≈100 mW cm^{-2}).

Microgel Sorting: Cell membranes were fluorescently labeled with 0.5% (v/v) Vybrant DiO. Microgels were sorted using a FACSAria II, which was controlled by FACSDiva software. Gate settings were determined after acquiring 50 000 data points.

Single-Cell-Laden Microgel Visualization: For SEM and FIB analyses, cell-laden microgels were dehydrated using graded ethanol series and liquid tert-butanol followed by liquid nitrogen freezing and sublimation using a cooled vacuum exicator. The microgels were then gold-sputtered and imaged using SEM or milled and then imaged using FIB/SEM. SEM photos of microgels embedded in agarose were pseudo-colored using Photoshop CS6 software. For fluorescent confocal microscopy, we made use of the microgels' permselectivity. 70 kDa dextran-fluorescein isothiocyanate (FITC) was added to the microgel suspension, allowing digital green coloring of the gels by inverting the green channel using ImageJ software. Alternatively, microgels were directly fluorescently labeled by incorporating dextran-FITC in the microgel precursor solution.

Permselectivity: Microgels were incubated with FITC-labeled dextran with molecular weights ranging from 10 to 70 kDa and proteins (bovine serum albumin and immunoglobulin G) for 6 d, after which the fluorescent intensities across the microgels were quantified using ImageJ software.

Biofabrication of 3D Modular Constructs: 3D modular constructs were produced by mixing PEGDA microgels into agarose, PEGDA, dextran-tyramine, collagen, alginate/GelMA, and alginate gel precursor solutions and subsequent processing using a variety of biofabrication techniques. The microgels' permselectivity enabled the exclusive FITC and rhodamine labeling (70 kDa dextran-FITC and dextran-rhodamine B isothiocyanate) of the macrogels. All 3D modular constructs were visualized using fluorescent confocal imaging and microphotography under UV light.

Supporting Information

Supporting Information is available from the Wiley Online Library or from the author.

Acknowledgements

M.K. and J.L. contributed equally to this work. The authors gratefully acknowledge the funding from the Dutch Arthritis Foundation (Grant No. 12-2-411 to J.L. and M.K. and a long-term program grant to M.K.). J.L. acknowledges financial support from Innovative Research Incentives Scheme Veni (Grant No. 14328) from the Netherlands Organization for Scientific Research (NWO). The authors thank the Medical Cell BioPhysics group (MIRA Institute for Biomedical Technology and Technical Medicine, University of Twente) for use of their flow cytometer. The authors thank H. A. G. M. van Wolferen for his expertise in FIB milling (MESA+ Institute for Nanotechnology, University of Twente). The authors acknowledge Hans Roerink BV, A. P. Bergink, and A. J. S. Renard (Ziekenhuisgroep Twente) for providing biological samples.

Received: August 15, 2016
Revised: November 11, 2016
Published online:

[1] J. S. Liu, Z. J. Gartner, *Trends Cell Biol.* **2012**, *22*, 683.
[2] a) L. Macri, D. Silverstein, R. A. Clark, *Adv. Drug Delivery Rev.* **2007**, *59*, 1366; b) P. A. Hall, F. M. Watt, *Development* **1989**, *106*, 619.
[3] S. J. Hollister, W. L. Murphy, *Tissue Eng., Part B* **2011**, *17*, 459.
[4] a) Y. Du, M. Ghodousi, H. Qi, N. Haas, W. Xiao, A. Khademhosseini, *Biotechnol. Bioeng.* **2011**, *108*, 1693; b) R. Tiruvannamalai-Annamalai, D. R. Armant, H. W. Matthew, *PLoS One* **2014**, *9*, e84287; c) A. P. McGuigan, M. V. Sefton, *Proc. Natl. Acad. Sci. USA* **2006**, *103*, 11461; d) N. Huebsch, E. Lippens, K. Lee, M. Mehta, S. T. Koshy, M. C. Darnell, R. M. Desai, C. M. Madl, M. Xu, X. Zhao, O. Chaudhuri, C. Verbeke, W. S. Kim, K. Alim, A. Mammoto, D. E. Ingber, G. N. Duda, D. J. Mooney, *Nat. Mater.* **2015**, *14*, 1269; e) V. E. Santo, A. R. Duarte, E. G. Popa, M. E. Gomes, J. F. Mano, R. L. Reis, *J. Controlled Release* **2012**, *162*, 19; f) R. Levato, J. Visser, J. A. Planell, E. Engel, J. Malda, M. A. Mateos-Timoneda, *Biofabrication* **2014**, *6*, 035020.
[5] S. Selimovic, J. Oh, H. Bae, M. Dokmeci, A. Khademhosseini, *Polymers* **2012**, *4*, 1554.
[6] a) D. M. Headen, G. Aubry, H. Lu, A. J. Garcia, *Adv. Mater.* **2014**, *26*, 3003; b) T. Rossow, J. A. Heyman, A. J. Ehrlicher, A. Langhoff, D. A. Weitz, R. Haag, S. Seiffert, *J. Am. Chem. Soc.* **2012**, *134*, 4983; c) T. Ashida, S. Sakai, M. Taya, *Artif. Cells, Nanomed., Biotechnol.* **2016**, *44*, 1406; d) W. H. Tan, S. Takeuchi, *Adv. Mater.* **2007**, *19*, 2696.
[7] a) A. Kumachev, J. Greener, E. Tumarkin, E. Eiser, P. W. Zandstra, E. Kumacheva, *Biomaterials* **2011**, *32*, 1477; b) Y. Ma, M. P. Neubauer, J. Thiele, A. Fery, W. T. S. Huck, *Biomater. Sci.* **2014**, *2*, 1661.
[8] a) S. Allazetta, L. Kolb, S. Zerbib, J. Bardy, M. P. Lutolf, *Small* **2015**, *11*, 5647; b) T. Aikawa, T. Konno, M. Takai, K. Ishihara, *Langmuir* **2012**, *28*, 2145.
[9] a) B. K. Mann, A. S. Gobin, A. T. Tsai, R. H. Schmedlen, J. L. West, *Biomaterials* **2001**, *22*, 3045; b) J. J. Moon, S. H. Lee, J. L. West, *Biomacromolecules* **2007**, *8*, 42; c) B. K. Mann, R. H. Schmedlen, J. L. West, *Biomaterials* **2001**, *22*, 439; d) M. P. Lutolf, J. L. Lauer-Fields, H. G. Schmoekel, A. T. Metters, F. E. Weber, G. B. Fields, J. A. Hubbell, *Proc. Natl. Acad. Sci. USA* **2003**, *100*, 5413.
[10] a) S. L. Anna, H. C. Mayer, *Phys. Fluids* **2006**, *18*, 121512; b) P. Garstecki, H. A. Stone, G. M. Whitesides, *Phys. Rev. Lett.* **2005**, *94*, 164501.
[11] C. Holtze, A. C. Rowat, J. J. Agresti, J. B. Hutchison, F. E. Angile, C. H. Schmitz, S. Koster, H. Duan, K. J. Humphry, R. A. Scanga, J. S. Johnson, D. Pisignano, D. A. Weitz, *Lab Chip* **2008**, *8*, 1632.
[12] C. L. Franco, J. Price, J. L. West, *Acta Biomater.* **2011**, *7*, 3267.
[13] a) A. Alhadlaq, J. H. Elisseeff, L. Hong, C. G. Williams, A. I. Caplan, B. Sharma, R. A. Kopher, S. Tomkoria, D. P. Lennon, A. Lopez, J. J. Mao, *Ann. Biomed. Eng.* **2004**, *32*, 911; b) B. Dhariwala, E. Hunt, T. Boland, *Tissue Eng.* **2004**, *10*, 1316.
[14] D. J. Collins, A. Neild, A. deMello, A. Q. Liu, Y. Ai, *Lab Chip* **2015**, *15*, 3439.
[15] E. W. M. Kemna, R. M. Schoeman, F. Wolbers, I. Vermes, D. A. Weitz, A. van den Berg, *Lab Chip* **2012**, *12*, 2881.
[16] a) E. Tumarkin, L. Tzadu, E. Csaszar, M. Seo, H. Zhang, A. Lee, R. Peerani, K. Purpura, P. W. Zandstra, E. Kumacheva, *Integr. Biol.* **2011**, *3*, 653; b) C. Y. Li, D. K. Wood, J. H. Huang, S. N. Bhatia, *Lab Chip* **2013**, *13*, 1969.
[17] Y. J. Eun, A. S. Utada, M. F. Copeland, S. Takeuchi, D. B. Weibel, *ACS Chem. Biol.* **2011**, *6*, 260.
[18] N. C. Hunt, L. M. Grover, *Biotechnol. Lett.* **2010**, *32*, 733.
[19] a) U. Del Monte, *Cell Cycle* **2009**, *8*, 505; b) T. M. Quinn, H. J. Hauselmann, N. Shintani, E. B. Hunziker, *Osteoarthritis Cartilage* **2013**, *21*, 1904; c) C. C. Miller, G. Godeau, C. Lebreton-DeCoster, A. Desmouliere, B. Pellat, L. Dubertret, B. Coulomb, *Exp. Dermatol.* **2003**, *12*, 403.
[20] T. C. Hales, *Ann. of Math.* **2005**, *162*, 1065.

[21] a) I. Vajanto, T. T. Rissanen, J. Rutanen, M. O. Hiltunen, T. T. Tuomisto, K. Arve, O. Narvanen, H. Manninen, H. Rasanen, M. Hippelainen, E. Alhava, S. Yla-Herttuala, *J. Gene Med.* **2002**, *4*, 371; b) E. J. Carragee, E. L. Hurwitz, B. K. Weiner, *Spine J.* **2011**, *11*, 471.
[22] S. Matsumoto, *J. Diabetes Metab. J.* **2011**, *35*, 199.
[23] S. Reardon, *Nature* **2015**, *527*, 152.
[24] a) G. M. Cruise, O. D. Hegre, F. V. Lamberti, S. R. Hager, R. Hill, D. S. Scharp, J. A. Hubbell, *Cell Transplant.* **1999**, *8*, 293; b) C. P. Pathak, A. S. Sawhney, J. A. Hubbell, *J. Am. Chem. Soc.* **1992**, *114*, 8311.
[25] E. S. Avgoustiniatos, C. K. Colton, *Ann. N. Y. Acad. Sci.* **1997**, *831*, 145.
[26] B. Ma, J. C. Leijten, L. Wu, M. Kip, C. A. van Blitterswijk, J. N. Post, M. Karperien, *Osteoarthritis Cartilage* **2013**, *21*, 599.
[27] S. K. Both, A. J. van der Muijsenberg, C. A. van Blitterswijk, J. de Boer, J. D. de Bruijn, *Tissue Eng.* **2007**, *13*, 3.